# Electron density topology of high-pressure $Ba_8Si_{46}$ from a combined Rietveld and maximum-entropy analysis

John S. Tse,[1,2] Roxana Flacau,[2] Serge Desgreniers,[2] Toshiaki Iitaka,[3] and J. Z. Jiang[4]
[1]*Department of Physics and Engineering Physics, University of Saskatchewan, Saskatoon, Saskatchewan, Canada S7N 5E2*
[2]*Laboratoire de Physique des Solides Denses, Department of Physics, University of Ottawa, Ottawa, Ontario, Canada K1N 6N5*
[3]*Computational Astrophysics Laboratory, RIKEN, 2-1 Hirosawa, Wako, Saitama 351-0198, Japan*
[4]*International Center for New-Structured Materials (ICNSM) and Laboratory of New-Structured Materials, Department of Materials Science and Engineering, Zhejiang University, Hangzhou 310027, People's Republic of China*
(Received 22 January 2007; revised manuscript received 22 May 2007; published 15 November 2007)

Under pressure, $Ba_8Si_{46}$ is found to undergo an isostructural transition, as observed by Raman spectroscopy, extended x-ray-absorption fine structure, and x-ray diffraction. Rietveld analysis of the x-ray diffraction data shows a homothetic contraction of the host lattice after the structural transition at 17 GPa. Using the Rietveld and maximum-entropy methods, we have performed an analysis of high resolution x-ray diffraction patterns collected from ambient to 30 GPa obtained in a diamond anvil cell using He as a quasihydrostatic pressure transmitting medium. The results indicate unambiguously that the homothetic phase transition at about 17 GPa is due to an extensive rehybridization of the Si atoms leading to a transfer of valence electrons from the bonding to the interstitial region. Consequently, the Si–Si bonds are weakened substantially at high density, leading to an abrupt collapse of the unit cell volume without a change in crystalline structure. The transition pressure and the change in the chemical bonding are remarkably similar to that observed in elemental Si–V.

DOI: 10.1103/PhysRevB.76.174109 PACS number(s): 61.50.Ks, 61.10.Nz, 71.20.Nr

## INTRODUCTION

Since the first report on the superconducting behavior of $Ba_8Si_{46}$, the properties of this compound and other related semiconductor clathrates have been studied extensively.[1–13] In addition to presenting a superconducting state, $Ba_8Si_{46}$ shows a peculiar physical property: when compressed, as shown from x-ray diffraction (XRD) measurements, a reversible isostructural phase transition occurs and is characterized by a sudden reduction in the unit cell volume at about 14–17 GPa.[13,14] In contrast to the change of the lattice parameter, no abrupt change in the atom positions has been found. Near-edge x-ray-absorption[13] and Raman spectroscopy studies,[10] however, have revealed an additional "transition" for $Ba_8Si_{46}$ at about 5 GPa. The physical origin of the two transitions, at 5 and 14–17 GPa, is still not clearly understood. The Ba $L_{III}$ x-ray appearance in near-edge spectroscopy spectra[13] show significant changes in the absorption edge position at 5 GPa, which might indicate rehybridization of the Ba atoms. However, except for the large volume collapse, there is no "electronic" or "structural" indication that may help characterize the second transition at about 17 GPa. To further explore the subtle changes in structural parameters and electronic density distribution induced by the application of high pressure, we have recently carried out high quality high-pressure angle-dispersive x-ray powder diffraction measurements on $Ba_8Si_{46}$ clathrate using He as a hydrostatic pressure transmitting medium.[14] Reliable structural parameters including thermal parameters were determined from Rietveld refinements. A significant finding of the previous study[14] is the anomalous behavior of the thermal parameters observed for Ba and Si atoms. At high pressure, it is generally expected that the atomic isotropic thermal parameter should decrease with increasing pressure. On the contrary, for $Ba_8Si_{46}$, it was found that for both Si and Ba, the isotropic thermal parameters increased at 5 GPa, at which pressure an apparent transition has taken place.[10] Additionally and more surprisingly, the Si thermal parameters were found to increase dramatically at 17 GPa.[14] It should be emphasized that the thermal parameters extracted from Rietveld refinements need not truly represent thermally excited vibrational motions. Sometimes, they serve to mimic and reproduce the effect of the distribution of electron density around the average atom position. Thus, a larger thermal parameter could reflect a static disorder or a genuine change in the electron density due to rehybridization of the Si atoms. In fact, our theoretical calculations of the equation of state using a disordered $Ba_8Si_{43}$ model with defect sites at the Si-6*c* positions seem to support the existence of static disorder. As an increase of the thermal parameters was observed on all the Si sites in $Ba_8Si_{46}$, vacancies in the Si-6*c* sites alone cannot entirely explain the experimental observation. Moreover, no amorphous or crystalline high-pressure Si phases were detected in the XRD patterns.

The goal of this investigation is to differentiate the static disorder from rehybridization that can occur in high-density $Ba_8Si_{46}$. For this purpose, the application of a model-independent method to extract the electron density directly from the XRD diffraction data is pursued. Electron density maps of $Ba_8Si_{46}$ at high pressure are determined from an analysis using the combined Rietveld and maximum-entropy methods[15–19] (Rietveld/MEM) of synchrotron radiation powder XRD data. The Rietveld/MEM analysis has provided insights for the structures and chemical bonding in a variety of materials. It has been shown, in some cases, that MEM is superior over the conventional Fourier synthesis in the reconstruction of the electron density map even without disorder in the structures.[15]

 

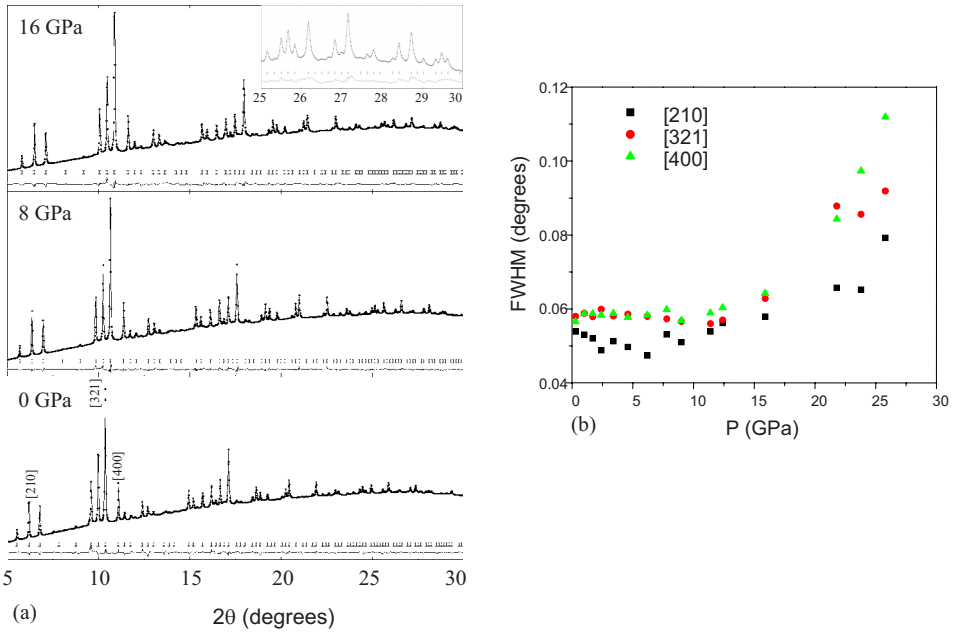


FIG. 1. (Color online) (a) (Left) Powder x-ray diffraction patterns of $Ba_8Si_{46}$ at selected pressures. The symbols denote the experimental data; the solid line, the calculated pattern; the thick marks, the calculated peak positions; and the bottom curve, the difference between observed and calculated patterns. Note the quality of the refinement and the fine details in the high-angle region (inset). (b) (Right) Change in the linewidth of selected Bragg reflections with pressure.

## EXPERIMENTAL DETAILS AND MAXIMUM-ENTROPY METHOD ANALYSIS

Alloy ingots with a composition of $Ba_8Si_{46}$ were prepared by arc melting pure elements of 99.9999% Si and 99.8% Ba in a purified argon atmosphere. Structure-I $Ba_8Si_{46}$ clathrate sample was synthesized by the high temperature and high-pressure route, as reported by Yamanaka *et al.*,[20] at 3 GPa and 1173 K using a multianvil pressure apparatus with 8 mm cube pressure cells.[21] Structure-I Si clathrate has a cubic space group with symmetry $Pm3n$, consisting of three unique Si atoms (Wyckoff positions 6*c*, 16*i*, and 24*k*) and two crystallographically distinct types of Ba atoms situated at Wyckoff symmetry positions 2*a* and 6*d*.[20] The Ba atoms hence occupy the centers of two small and six large cagelike units formed by Si atoms in the cubic structure-I clathrate.

High quality angle-dispersive x-ray diffraction (XRD) measurements at ambient temperature and at high pressure using a diamond anvil cell with He as the pressure transmitting medium were carried out at BL10XU beamline of SPring8 (Japan) with a wavelength of 0.4969 Å. Using an image plate detector, a total of 25 diffraction patterns were recorded from room pressure to approximately 32 GPa.

For the purpose of calculating the charge density distributions, the measured data were analyzed by the combination of Rietveld and MEM methods.[15–19] The details of the combined Rietveld/MEM analysis of powder XRD data have been presented extensively in the literature.[15–19] In short, MEM calculations use scaled, phased, "error-free" structure factors $[F_o(hkl)]$ as inputs for finding the numerical electron density at grid pixel $i$ ($\rho_i$) that optimizes the entropy function $S$ from a prior electron density at pixel $i$, $\tau_i$,

$$S = -\sum \rho_i \ln(\rho_i/\tau_i), \tag{1}$$

subject to the principle of conservation of the total charge density ($n_e/V$), i.e.,

$$n_e/V = \frac{1}{n}\sum \rho_i, \tag{2}$$

where $n$ is the total number of pixels in unit volume $V$, and under to the requirement that the observed and calculated structure factors agree within the $\chi^2$ test, i.e.,

$$\chi^2 = \frac{1}{N}\sum_{hkl} \frac{[F_{\mathrm{MEM}}(hkl) - F_o(hkl)]^2}{\sigma(hkl)^2} = 1, \tag{3}$$

where $N$ is the number of x-ray diffraction reflections and $\sigma(hkl)$ is the standard deviation for $F_o(hkl)$.

Conventional Rietveld refinements of XRD data are first used to extract structure factors from the synchrotron powder diffraction data. For that purpose, we used pseudo-Voigt line profiles, which reproduce well the x-ray diffraction data recorded at high pressure. For MEM refinements to be successful, well resolved XRD patterns are needed, particularly, at high diffraction angles.

XRD patterns (observed and calculated) of $Ba_8Si_{46}$ measured at 0.3, 7.8, and 16 GPa are shown in Fig. 1(a). The difference (residuals) traces illustrate the good quality of XRD data and refinements. Even at high pressure, the Bragg reflections at high angles (e.g., $25° < 2\theta < 30°$) are clearly resolved. Linewidths of three nonoverlapping reflections obtained from the refinements are shown in Fig. 1(b). Importantly, no deterioration of both the line shape and linewidth [full width at half maximum (FWHM)] was observed up to 16 GPa, a result of using He as a hydrostatic pressure transmitting medium. At higher pressure, a substantial broadening of the width of all the Bragg peaks is observed. Moreover, the FWHM increases with increasing pressure. The abrupt change in the x-ray diffraction peak profile is obviously intrinsic to the phase transition since the He pressure medium is expected to remain hydrostatic at least up to 30 GPa. It is worth mentioning that we have assumed that the physical properties of $Ba_8Si_{46}$ and the observed x-ray diffraction are

not affected by intercalation of He atoms in $Ba_8Si_{46}$ at high pressure, if present at all. Observed structure factors, derived from the Rietveld analysis [RIETAN-2000 Refs. 16 and 22], were subsequently used for MEM calculations, as carried out using PRIMA.[17,22] The total number of reflections considered in the MEM analysis varied from 129 (at 0.3 GPa) to 95 (at 25.8 GPa). Out of the total number, 43 and 40 reflections were nonoverlapping for 0.3 and 25.8 GPa, respectively. It should be noted that the relatively short range in $\sin(\theta)/\lambda$, smaller than about 1 $Å^{-1}$ in our case, is compensated by the large number of $(hkl)$ reflections resulting from the large lattice parameter of cubic structure I. The reliability factors $R_{wp}$ and $R_I$ for the Rietveld refinements were, typically, 1.3% and 6%, respectively. MEM analyses were initiated from a uniform prior charge density distribution and performed for a cubic lattice of $64\times64\times64$ pixels. MEM analyses were followed by iterations of MEM-based pattern fitting[18] to minimize the bias to the structural model in the extraction of the observed structure factors $F_o(hkl)$. The iterative procedure was repeated until the $R_I$ factor was minimized, becoming 3% on average, as opposed to 6%, as obtained typically from a Rietveld refinement only. The weighted reliability factor ($R_{wp}$) derived from the MEM analysis was in the 2.5%–3.9% range for the data in the entire pressure measurements domain. The electron density maps were generated using programs LIMNER (Ref. 23) and XCRYSDEN.[24]

The use of MEM suffers from a problem inherent to any other methods used to reconstruct electron density distributions: the reliability of x-ray diffraction data is undoubtedly crucial in obtaining accurate electron density distribution in the vicinity of atomic. Nevertheless, MEM has been shown to be particularly useful to retrieve information from imperfect, i.e., as in being incomplete or/and with noise.[15] The reliability of MEM in generating accurate electron density distribution has been discussed.[25,26] The powder x-ray diffraction data presented here are to be considered "imperfect" although of best quality, given that they were obtained from clathrate samples submitted to high pressures, and we advance that the Rietveld/MEM, as presented in this paper, should at least give a significant estimation of the evolution with density of structural parameters and electronic density distribution. Previously, MEM has been used to extract the neutron density of proton disordered structure-I hydrate,[27] which has the same structure as the $B_8Si_{46}$ clathrate;[20] results were judged in excellent agreement as compared to those derived using a more conventional multipole refinement.

## RESULTS AND DISCUSSION

The Rietveld/MEM refinements reproduce structure and electron density variations which, as we advance, are in relation to the structural changes reported in the two earlier studies.[9,13] Before developing an understanding of the change of electron density topology of $Ba_8Si_{46}$ under pressure, it is worthy to study the charge density difference $[\Delta\rho=\rho(P)-\rho(0)]$ between the calculated charge density at a given pressure, $\rho(P)$, relative to that at the lowest pressure (0.3 GPa, in our study), $\rho(0)$, as obtained from MEM analysis. The $\Delta\rho$ maps were computed from subtraction of the charge density at each grid point used in the MEM analysis. Therefore, the effect of volume reduction at higher pressures was not taken into account. The purpose of this comparison is (i) to establish internal consistency of the electron density computed using Rietveld/MEM from the inspection of the electron density changes as a function of pressure and (ii) to provide qualitative information on the change of electron density topology when $Ba_8Si_{46}$ is compressed, even without proper volume normalization.

Regarding the uncertainty of electron density maps constructed from the probability distribution as obtained from the MEM analysis, most of the uncertainty in electron density arises from (1) using nonideal x-ray diffraction sets obtained from sample nonambient conditions, i.e., at high pressure, (2) $\sin(\theta)/\lambda$ limited data sets, and (3) the difficulty in extracting and accounting for structure factors corresponding to overlapping $(hkl)$ reflections. Additionally, to a lesser extent, the MEM procedure itself also accounts for part of the uncertainty.[26] The effect of limited reciprocal space covered by conventional x-ray diffraction data has been discussed by Merli and Pavese:[25] a substantial improvement in recovering good electron density results from MEM has been shown for x-ray diffraction data for MgO covering values above $\sin(\theta)/\lambda>1$ $Å^{-1}$, corresponding to a number of observed reflections of about 40. Furthermore, as demonstrated in the thorough study on MgO, the lack of high-angle data affects mostly the core electron density and does not alter the valence electron distribution severely.[25] For the present case, at all pressures, the x-ray diffraction data although covering values corresponding to $\sin(\theta)/\lambda>0.5$ $Å^{-1}$, the total number of observed reflections, typically more than 100 given the relatively large dimension of the cubic unit cell, were considered sufficient. At all pressures, we have found a good agreement between the observed and the calculated (by Rietveld/MEM) structure factors for all $(hkl)$ reflections. The distribution of the normalized residuals, $[F_{MEM}(hkl)-F_o(hkl)]/\sigma_o(hkl)$, indicates that most of the structure factors reconstructed by the Rietveld/MEM analysis fall within about $1.5\sigma$, as compared to the observed structure factors. Results for selected pressures (0.3 and 21.8 GPa) are illustrated in Fig. 2 (top). All data points corresponding to a deviation of more than 10% in $[F_{MEM}(hkl)-F_o(hkl)]/F_o(hkl)$, as shown in Fig. 2 (bottom), correspond, in fact, to overlapping $(hkl)$ reflections for which the corresponding $F_o(hkl)$ have larger errors. Uncertainties in electron density reconstructed by MEM have been shown to vary from 16% to 31% at the smallest electron density regions for case of the best powder x-ray diffraction data of Si and a small and incomplete x-ray data set for CuBr, respectively.[26] Similarly, for the present study, we estimate the errors in the calculated $F_{MEM}(hkl)$, both statistical and systematic, to translate to electron density uncertainties ranging from 5% to less than 30%, the largest uncertainties being associated with lowest electron density reconstructed in the atomic bonding regions and the smallest for those obtained for the largest "core" electron density in the vicinity of atomic sites. Although the uncertainties associated with the reconstructed electron density may be considered relatively large, we argue that a change in electron density can still be observed as a

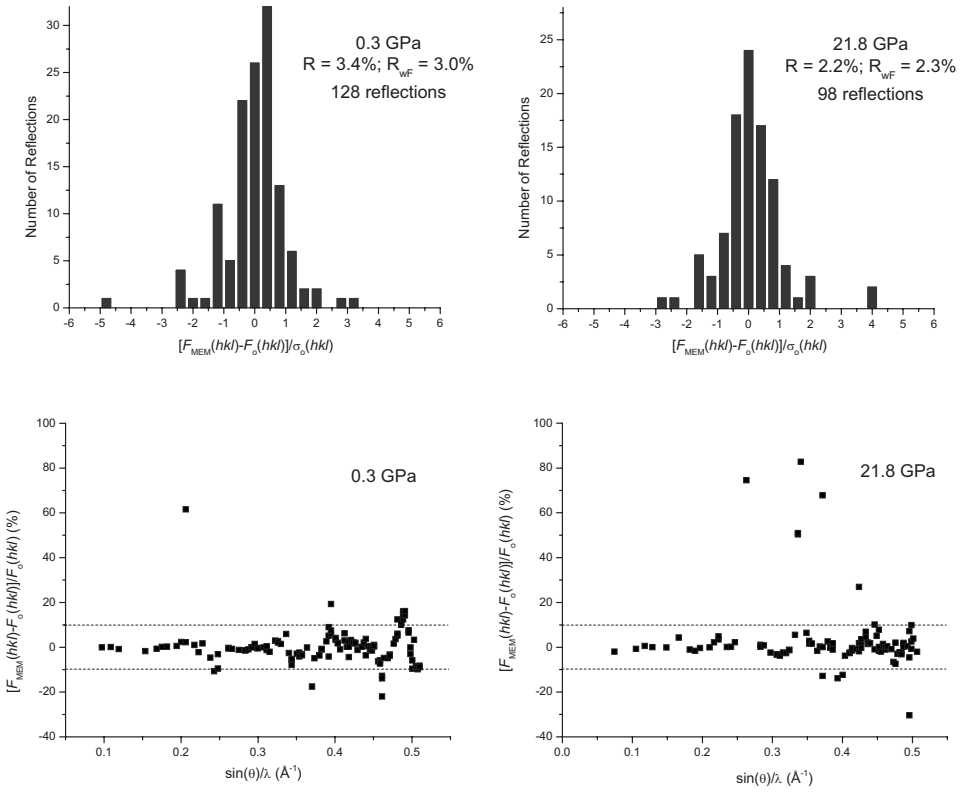


FIG. 2. (Top left and top right) Histogram of normalized structure factor residuals, $[F_{\mathrm{MEM}}(hkl) - F_o(hkl)]/\sigma_o(hkl)$, for all $(hkl)$ reflections recorded in $Ba_8Si_{46}$ at low and high pressures, i.e., 0.3 and 21.8 GPa. (Bottom left and bottom right) Structure factor residuals, $[F_{\mathrm{MEM}}(hkl) - F_o(hkl)]/F_o(hkl)$, as a function of scattering angle. All data points outside the ±10% margins correspond to observed structure factors $F_o(hkl)$ for overlapping $(hkl)$ reflections for which the respective error is large.

function of increasing density induced by the application of pressure in $Ba_8Si_{46}$ and a comparison between electron density distributions reconstructed at different pressure is worth doing, as we present next.

Figure 3 (bottom) shows charge density difference maps at selected pressures for the (200) plane. The (200) plane cuts through the middle of the cubic unit cell and displays the charge density of Ba atoms in the small cages (Ba-*S*) together with those of Si atoms at positions $24k$ $(0,y,z)$ and $6c$ $(\frac{1}{4},0,\frac{1}{2})$, which are forming the clathrate framework. Systematic changes in the charge density differences are observed. The appearance of systematic changes demonstrates the internal consistency of the charge density derived from the MEM analysis. At pressures below 9 GPa, electrons are polarized away from the Ba central sites in the small cages $(\frac{1}{2},\frac{1}{2},\frac{1}{2})$, as indicated by a slight depletion of charge density (Fig. 3, dark) at the Ba $2a$ sites, into the immediate surrounding (Fig. 3, light). There are also significant charge accumulations on the framework Si atoms. From 9 to 16 GPa, again relative to the 0.3 GPa, a gradual charge transfer is observed from both the Si and the Ba atoms into the interstitial space. As only a section of the (200) plane is illustrated in Fig. 3 (bottom), Ba atoms in the large cages (Ba-*L*), which are situated at the edges $(0,\frac{1}{4},\frac{1}{2})$ and $(0,\frac{3}{4},\frac{1}{2})$, are not readily visible. To better visualize the change in Ba-*L* charge density, the (100) plane is plotted in Fig. 3 (top); in this case, Ba atoms are located in the middle of the plane. Similarly, a systematic change in the charge density difference contours is observed relative to the charge density at 0.3 GPa. The most noticeable feature is the gradual increase in the charge accumulation on the Si atoms for pressures up to 7.8 GPa. In contrast to the situation for Ba-*S*, there is a significant accumulation of electrons at the Ba-*L* sites. As pressure is increasing over 7.8 GPa, the charge accumulation relative to the 0.3 GPa distribution at the Si sites starts to diminish. At 16 GPa, the electron distribution at the Si atoms is depleted quite significantly. It is also evident from the charge density difference plots that from 9 to 16 GPa, the Si-6*c*, Si-24*k*, and Ba-*L* atomic positions become disordered and displaced from their respective crystallographic symmetry sites. This observation is consistent with the sudden increase in atomic thermal parameters determined from previous Rietveld refinements[14] and the observed increase of the Bragg reflection linewidths at the same pressure range.

A picture of the charge density redistribution in $Ba_8Si_{46}$ due to compression emerges from the survey of the charge difference maps. Ba atoms in the small cages are more susceptible to sharing valence electrons with cage forming Si atoms when cubic structure-I $Ba_8Si_{46}$ is compressed. There is an initial accumulation of electrons on the framework Si atoms until 7 GPa. Between 7 and 16 GPa, the charge redistribution on the Si atoms seems to decrease, and then the electron charge starts to shift away from the Si atoms for pressures higher than 16 GPa. The electron density of the Ba atoms in the large cages seems to accumulate and distort significantly with increase pressure. The distortion of the electron cloud around the Ba-*L* atom shows that the electrons are polarized away from the ideal crystallographic atomic sites. The analysis of the electron density distribution reveals that there are clear signs of pressure induced electronic changes at about 7 GPa and at 16 GPa. As will be further discussed below, the changes in electron density distribution are related to the phase transitions observed in $Ba_8Si_{46}$.

The electron density maps computed from the Rietveld/MEM analysis cutting through the two unique Ba atoms

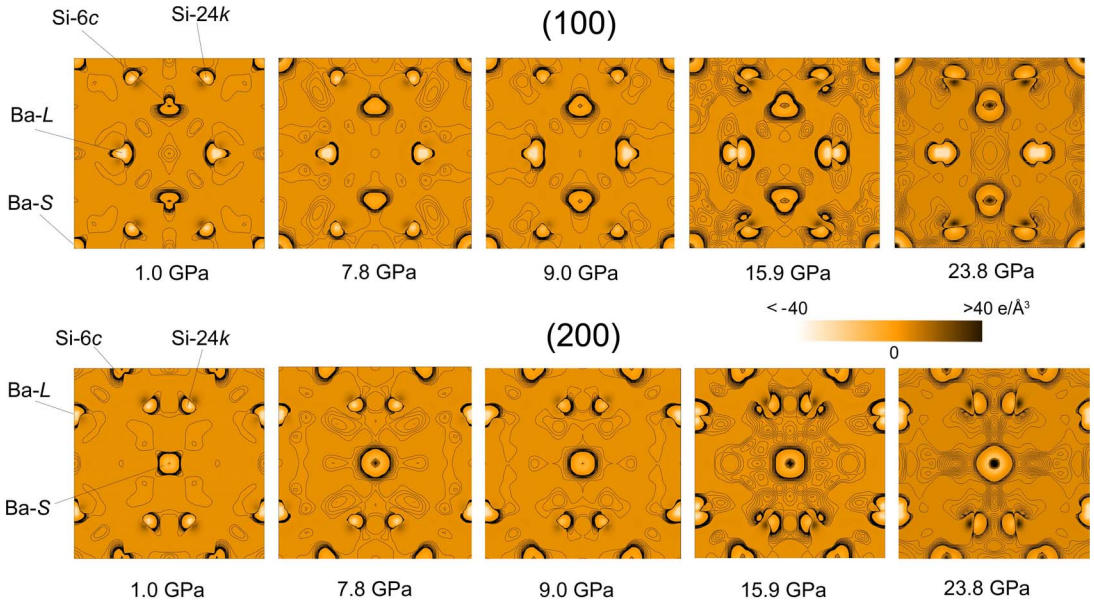


FIG. 3. (Color online) Plots of Rietveld/MEM charge density difference relative to 0.3 GPa at selected pressures. The color scale is in $e/\text{Å}^3$. Contour lines are drawn at every 0.1 $e/\text{Å}^3$. Note that the charge densities at high pressures are not normalized to the volume change (see text).

[(100) and (200)] and pairs of Si bonds (in (110)) at 1, 9, 16, and 22 GPa, bracketing the observed phase transitions at 6–7 and 15–17 GPa, are shown in Figs. 4–6, respectively. The results are in substantial agreement with the preliminary assessments from the charge density difference plots depicted in Fig. 3. The contour lines around the two Ba-*L* atoms lying on the (100) plane clearly show that at low pressure (1 GPa), the electron densities are mostly concentrated in close proximity to atom centers. As the pressure increases, e.g., to 9 GPa, the electron density becomes more diffuse and spreads over into the interstitial space. There is also a strong indication that the "effective" size (indicated by the high-density region) of the Ba was somewhat reduced. Moreover, the contour lines around the Si atoms become denser, indicating a small increase in charge accumulation. A similar charge distribution pattern also emerges for the Ba-*S* atom lying in the (200) plane when $Ba_8Si_{46}$ is compressed from 1 to 9 GPa. A substantial charge transfer from the Ba atoms to the Si framework under ambient pressure is already present. This observation indicates that Ba-Si interactions are enhanced upon compression and promote the migration of Ba valence electrons into empty states of predominant Si

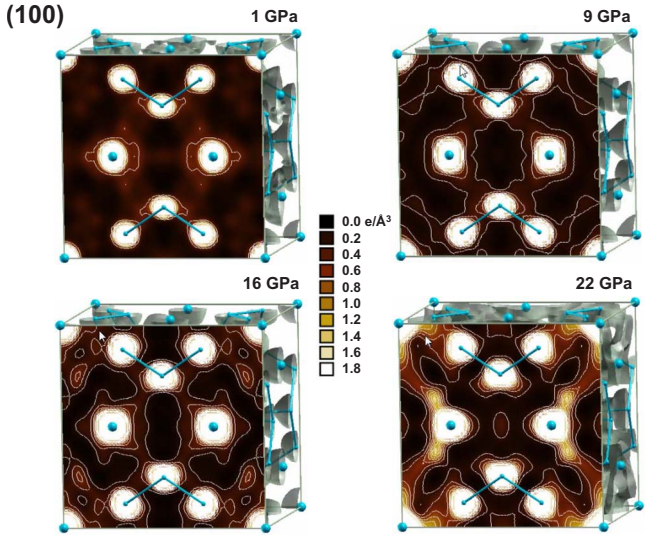


FIG. 4. (Color online) Contour plots of the charge density derived from Rietveld/MEM analysis of $Ba_8Si_{46}$ in the (100) plane at selected pressures, highlighting the Ba atom in the large cage. The unit of the contour lines is 0.1 $e/\text{Å}^3$.

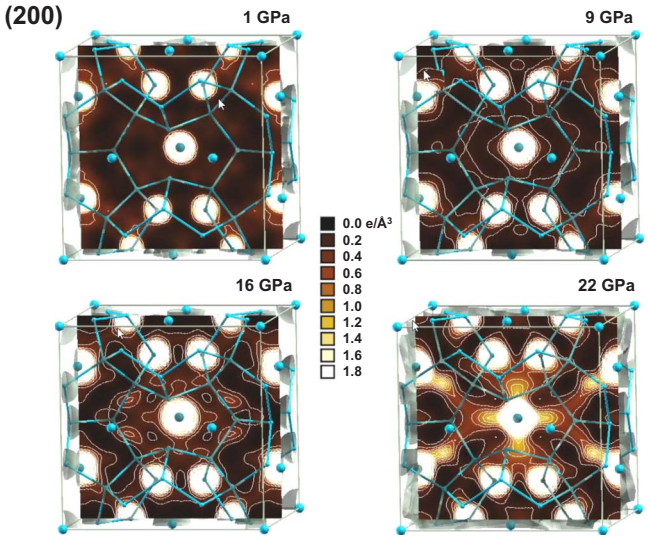


FIG. 5. (Color online) Contour plots of the charge density derived from Rietveld/MEM analysis of $Ba_8Si_{46}$ in the (200) plane at selected pressures, highlighting the Ba atom in the small cage. The unit of the contour lines is 0.1 $e/\text{Å}^3$.

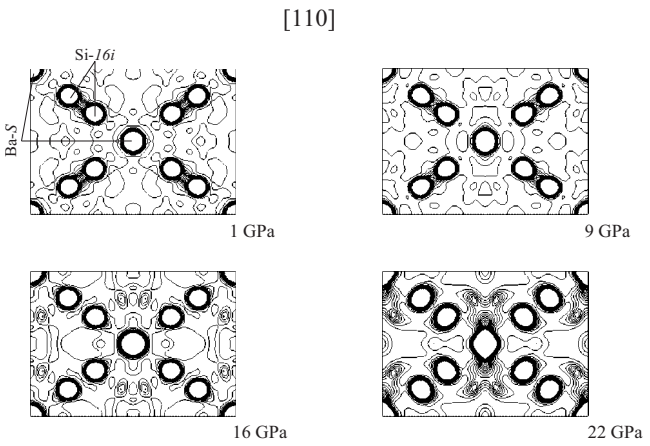


FIG. 6. Two-dimensional contour plot of the charge density derived from Rietveld/MEM analysis of $Ba_8Si_{46}$ in the (110) plane at selected pressures highlighting the Si–Si bonds. The electron density limits are 0.1 and 2.0 $e/Å^3$ with a contour spacing of 0.1 $e/Å^3$.

character. This behavior is consistent with the calculated electronic band structure of $Ba_8Si_{46}$, which reveals that strong hybridization of the Ba state with the $Si_{46}$ conduction band plays a key role in the superconducting behavior.[28–30] The increase of charge density in the interstitial region and at the Si atoms sites is in accord with the increase of the atomic thermal parameters determined from the previous study based on a Rietveld refinement.[14]

When $Ba_8Si_{46}$ is compressed beyond 16 GPa, a dramatic change in the electron topology around the Ba atoms is observed. The electron density around the Ba atoms, both in the small and large cages, distorts from the atomiclike spherical distribution. In the (200) plane (Fig. 5), electrons around the Ba-*S* atom extend toward the Si atoms and to the nearest neighbor Ba-*L* atoms in adjacent cages. There are signs of significant overlap of the valence electrons from the Si and both types of Ba atoms. This is a consequence of the valence electrons from these atoms being "squeezed" into the interstitial space. A very similar electron density topology is also observed for the Ba atom in the large cage [the (100) plane as shown in Fig. 4] although to a lesser extent.

The remaining question is as follows: "Why and where the electrons have gone as the Si atom sites get depleted at high pressure?" To answer this point, the electron density maps at different pressures in the (110) plane are compared in Fig. 6. The (110) plane was chosen as it shows the projection of the charge density of the Si bonds between two connecting symmetry related Si atoms at 16*i* sites. At 1 GPa, the electron density is found to concentrate between the Si atoms, indicating strong genuine $\sigma$-covalent bonds. As the pressure is increased, the electron density distribution between the two bonded Si atoms becomes more diffuse and delocalized into the open space. A more significant change is observed at pressure above 16 GPa. The electron density is no longer concentrated between the Si atoms but is squeezed into the interstitial space. The electron topology clearly shows a reduction in the $\sigma$ character of the Si–Si bond and replacement by mostly $\pi$-bonding-like interactions.

The extensive distortion of valence electron density distribution from 16 to 22 GPa signifies, unambiguously, an electron topological transition as the crystal symmetry remains unaltered. The onset of the delocalization of valence electrons coincides with the sudden increase in the thermal parameters of Si and Ba atoms at 17 GPa observed in previous Rietveld refinements.[14] Incidentally, the transition pressure of 17 GPa is almost identical to the recently observed *direct* transformation from face centered cubic (*cF*8) Si (ambient structure) to Si–V (a phase at 17 GPa and room temperature).[31] Under quasihydrostatic conditions at low temperature, it was found that the *cF*8 Si phase is indeed metastable. As a matter of consequence, the intermediate $\beta$-tin and orthorhombic high-pressure structures are bypassed and a phase transformation takes place directly to the Si–V at 17 GPa. It is worth mentioning that *cF*8 Si is composed of perfect tetrahedrally coordinated Si atoms, whereas the Si–V phase is metallic and consists of rows of Si linear chains.[32] In the latter case, a strong mixing of Si 3*d* with *s-p* valence orbitals results in a transfer of "bonding" valence electrons into the interstitial space and, as a result, the rehybridization leads to weakened Si–Si bonds.[32] Therefore, the phase transition to the Si–V phase is associated with a very large volume reduction.

A similar scenario can be invoked to rationalize the observed change in electron topology in $Ba_8Si_{46}$ under pressure. As pressure is increased to 7 GPa, the initial response of the system is to bring the Ba and Si atoms closer. As a result, there is some enhancement of charge transfer from the Ba to the Si framework; this results in small charge depletion in Ba located in small cages and slight charge accumulation at the Si atoms. As pressure increases further, the electron density delocalizes into the interstitial region. The $\pi$-bonding-like electron topology derived from Rietveld/MEM analysis is a clear evidence of strong *spd* hybridization.[32] The possibility of Ba hybridization in Si clathrate was already raised.[33] Thus, under very high pressure, the Si atoms utilize the more diffuse *d* states to redistribute the bonding electrons into the more open but less repulsive space and, at the same time, weaken the Si–Si bonds, resulting in a contraction of the volume during this electron topological homothetic phase transition.

The conclusions drawn from the Rietveld/MEM analysis are in accord with experimental observations. The explanation of the Raman[10] and extended x-ray-absorption fine structure[13] (EXAFS) spectra of $Ba_8Si_{46}$ at the low-pressure region (below 16 GPa) is similar to that offered in a previous study. It was shown, from the EXAFS study,[13] that the energy of the Ba $L_{III}$ absorption edge first increases with pressure and then decreases suddenly, showing a discontinuity at 5 GPa. The increase in the energy of the inflection point of the white line can be rationalized as the result of charge transfer of Ba atoms to the Si framework. It should be noted that both EXAFS and Raman are more sensitive to the changes in Ba or Ba-Si interactions in the large cages. From factor group analysis,[31] it is easy to show that Ba atom vibrations in the small cages are not Raman active. Moreover, it has been suggested that features in the Ba-*L*-absorption edge probably only probe changes of the large cages since there are three times more than small cages.[20] Examination of the electron density maps in the (100) plane indeed revealed that Ba atoms in large cages start to change the almost

spherical electron distribution at 6.2 GPa and become more anisotropic and "spread out" at higher pressures. A more positively charged Ba atom is expected to increase the excitation energies to the empty states. As suggested earlier,[14] a tighter Ba ion will be less polarizable, thus reducing the intensity of the Raman bands.

In a previous study,[14] two explanations were proposed to rationalize the volume reduction associated with the isostructural transition at 17 GPa. The observed phase transition in $Ba_8Si_{46}$ is first correlated to a similar pressure induced transition observed in pure *cF*8 Si to Si–V.[31,32] A sudden change in compressibility and volume contraction during the phase transition due to the creation of Si vacancies was invoked as another possible explanation.[35] The apparently good agreement between experimental and theoretical equations of state on a $Ba_8Si_{43}$ model with Si vacancies in the Si-6*c* sites at pressures over 17 GPa lends support to the latter explanation.[35] There are, however, several weaknesses to this proposal. Rietveld refinements[14] show no anomaly in the atom positions close to and after the phase transition. In addition, refinement of the Si site occupancies failed to converge to a reasonable structure solution. Moreover, anomalously large thermal parameters were observed at all Si positions and not restricted to Si at 6*c* sites. The proposed "disordered" structure mechanism also required the formation of "excess" Si that was excluded from the sample. As far as we can tell, there was no significant evidence from the XRD data to support this suggestion. Furthermore, there is no sudden change in the background of the powder x-ray diffraction patterns that might be attributed to the formation of amorphous silicon nor there are any additional Bragg peaks that otherwise could be assigned to any high-pressure phase of Si.

The direct analysis of experimental electron density distributions indicates that the observed phase transition at about 16–17 GPa is driven by a sudden change in the electron density topology due to a substantial rearrangement of the distribution of the valence electrons and is likely to be correct, as proposed before.[14] This is accompanied with disordering in the Si sites. The mechanism for this transition may be classified as a special case of the more general electron topological transition (ETT). An ETT transition is due the change in the topology of the Fermi surface due to changes in the occupations of the filled and empty bands at the vicinity of the Fermi level without a structural transformation. The observed redistribution of the electron density is consistent with the trend in the variation of the atomic thermal parameters with pressure reported recently.[14]

## CONCLUSIONS

Electron density distribution maps in $Ba_8Si_{46}$ from 0.3 to 23 GPa have been derived from Rietveld/MEM analysis of high resolution powder XRD patterns. The electron density maps show substantial changes in the distribution of the valence charge density at pressure above 17 GPa. Significantly, the electrons in the Si–Si bonds are removed from the bonding region into the interstitial region. The dramatic change in the electron density weakens the Si–Si bonds, resulting in a displacive but isostructural phase transition taking place with a large volume reduction. This electron topological transition shares the same physical origin with the *cF*8 Si→Si-V transition.[34] In both cases, strong mixings of Si valence 3*sp* with diffuse 3*d* orbitals help alleviate the repulsive interactions between electrons in the bonding region by delocalization into the interstitial region. As a consequence, the Si–Si bonds are weakened, resulting in a large volume collapse accompanying the phase transition. This interpretation also helps explain the Raman[10] and EXAFS[13] spectra and the anomalies observed in the atomic thermal parameters extracted from a previous Rietveld analysis. We would like to emphasize that the present work constitutes an attempt in interpreting the observation of a homothetic transition in Si clathrates by studying the change of electronic density using MEM under pressure. We recognized that even with the best effort, the quality of the x-ray diffraction data obtained from a sample submitted to high pressure with a diamond anvil cell is somewhat limited and, consequently, it may not represent the ideal test case for the reconstruction of accurate of electron density by the Rietveld/MEM. However, we believe that the change of the electron density topology observed in association with the phase transition at 17 GPa is genuine and correct. In high-pressure studies, the sensitivity to changes in the experiment is considerably more accurate than the absolute determination. In principle, this sensitivity can be evaluated from careful studies under pressure using the same method on reference samples. This is, however, very demanding on the synchrotron beam time. In this case, even if errors in the density maps are large, the change in the electron topology can be considered as fair enough to guarantee the interpretation of the physics on the volume collapse. There is a remaining problem: The observed change in electron density was not reproduced by first principles electronic structure studies reported previously. At this moment, we cannot offer a reasonable solution to resolve this discrepancy. More extended experimental and theoretical studies are needed to reconcile this apparent discrepancy.

## ACKNOWLEDGMENTS

J.S.T. and T.I. wish to thank RIKEN (Japan) for a generous allocation of computing resource on the RSCC system where all the theoretical electronic calculations were performed. J.S.T., R.F., and S.D. acknowledge the financial support of NSERC of Canada. J.Z.J. would like to thank SPring8 (Japan) for use of the synchrotron radiation facilities at beamline BL10XU (Proposal No. 2004A0603) and financial support from the National Natural Science Foundation of China (Grants No. 50341032, No. 50425102, No. 50601021, No. 5070138, and No. 60776014), the Ministry of Science and Technology of China (Grants No. 2004/249/37-14 and No. 2004/250/31-01A), the Ministry of Education of China (Program for Chiangjiang Scholars), Zhejiang University-Helmholtz cooperation fund, and Zhejiang University.

[1] H. Kawaji, H. Horie, S. Yamanaka, and M. Ishikawa, Phys. Rev. Lett. **74**, 1427 (1995).
[2] K. Tanigaki, T. Shimizu, K. M. Itoh, J. Teraoka, Y. Moritomo, and S. Yamanaka, Nat. Mater. **2**, 653 (2003).
[3] J. L. Cohn, G. S. Nolas, V. Fessatidis, T. H. Metcalf, and G. A. Slack, Phys. Rev. Lett. **82**, 779 (1999).
[4] J. S. Tse, K. Uehara, R. Rousseau, A. Ker, C. I. Ratcliffe, M. A. White, and G. MacKay, Phys. Rev. Lett. **85**, 114 (2000).
[5] J. Gryko, P. F. McMillan, R. F. Marzke, G. K. Ramachandran, D. Patton, S. K. Deb, and O. F. Sankey, Phys. Rev. B **62**, R7707 (2000).
[6] D. Connetable, V. Timoshevskii, E. Artacho, and X. Blase, Phys. Rev. Lett. **87**, 206405 (2001).
[7] A. San-Miguel, P. Kéghélian, X. Blase, P. Mélinon, A. Perez, J. P. Itié, A. Polian, E. Reny, C. Cros, and M. Pouchard, Phys. Rev. Lett. **83**, 5290 (1999).
[8] J. S. Tse, S. Desgreniers, Z. Q. Li, M. R. Ferguson, and Y. Kawazoe, Phys. Rev. Lett. **89**, 195507 (2002).
[9] A. San-Miguel, P. Mélinon, D. Connétable, X. Blase, F. Tournus, E. Reny, S. Yamanaka, and J. P. Itié, Phys. Rev. B **65**, 054109 (2002).
[10] T. Kume, H. Fukuoka, T. Koda, S. Sasaki, H. Shimizu, and S. Yamanaka, Phys. Rev. Lett. **90**, 155503 (2003).
[11] M. Wilson and P. F. McMillan, Phys. Rev. Lett. **90**, 135703 (2003).
[12] T. Kume, T. Koda, S. Sasaki, H. Shimizu, and J. S. Tse, Phys. Rev. B **70**, 052101 (2004).
[13] A. San Miguel, A. Merlen, P. Toulemonde, T. Kume, S. Le Floch, A. Aouizerat, S. Pascarelli, G. Aquilanti, O. Mathon, T. Le Bihan, J. P. Itié, and S. Yamanaka, Europhys. Lett. **69**, 556 (2005).
[14] L. Yang, Y. M. Ma, T. Iitaka, J. S. Tse, K. Stahl, Y. Ohishi, Y. Wang, R. W. Zhang, J. F. Liu, H.-K. Mao, and J. Z. Jiang, Phys. Rev. B **74**, 245209 (2006).
[15] M. Takata, E. Nishibori, and M. Sakata, Z. Kristallogr. **261**, 71 (2001).
[16] F. Izumi and T. Ikeda, Mater. Sci. Forum **321-324**, 198 (2000).
[17] F. Izumi and R. A. Dilanian, *Recent Research Developments in Physics* (Transworld Research Network, Trivandrum, 2002), Vol. 3, Pt. II, p. 669.
[18] F. Izumi and T. Ikeda, IUCr/CPD Newsletter **26**, 7 (2001).
[19] M. Fujimori, T. Nakata, T. Nakayama, E. Nishibori, K. Kimura, M. Takata, and M. Sakata, Phys. Rev. Lett. **82**, 4452 (1999).
[20] S. Yamanaka, E. Enishi, H. Fukuoka, and M. Ishikawa, Inorg. Chem. **39**, 56 (2000).
[21] J. Z. Jiang, W. Roseker, M. Sikorski, Q. P. Cao, and F. Xu, Appl. Phys. Lett. **84**, 1871 (2004).
[22] See http://homepage.mac.com/fujioizumi/visualization/VENUS.html
[23] Y. Shimizu and H. Tanaka, LIMNER v1.04—a 3D visualization program for charge density analysis using MEM. http://www.phys.shimane-u.ac.jp/tanaka_lab/programs/limner/limner.html
[24] Kokalj, J. Mol. Graphics Modell. **17**, 176 (1999); www.xcrysden.org
[25] M. Merli and A. Pavese, Z. Kristallogr. **221**, 613 (2006).
[26] L. Dobrzyński and J. Waliszewski, J. Phys. Soc. Jpn. **72**, 2203 (2003).
[27] J. Baumert, C. Gutt, M. R. Johnson, J. S. Tse, D. D. Klug, and W. Press, J. Chem. Phys. **120**, 10163 (2004).
[28] S. Saito and A. Oshiyama, Phys. Rev. B **51**, 2628 (1995).
[29] K. Moriguchi, M. Yonemura, A. Shintani, and S. Yamanaka, Phys. Rev. B **61**, 9859 (2000).
[30] J. S. Tse, T. Iitaka, T. Kume, H. Shimizu, K. Parlinski, H. Fukuoka, and S. Yamanaka, Phys. Rev. B **72**, 155441 (2005).
[31] J. S. Tse, C. I. Ratcliffe, B. M. Powell, V. F. Sears, and Y. P. Handa, J. Phys. Chem. A **101**, 4491 (1997).
[32] M. Hanfland (private communication); Abstract of the 12th International Conference of High Pressure Semiconductor Physics, Barcelona, 2006 (unpublished).
[33] A. San Miguel and P. Toulemonde, High Press. Res. **25**, 159 (2005).
[34] J. S. Tse, Z. Kristallogr. **220**, 521 (2005).
[35] T. Iitaka, Phys. Rev. B **75**, 012106 (2007).